Supplementary Information

Unveiling a conversion-intercalation dual mechanism in Cr-doped $TaSe_2$ electrodes for high-capacity primary-secondary lithium-ion batteries

Qianshuo Wang, [a] Yanhao Dong, [a] Tu Lan,*[a] Junke Ma, [a] Yongzhi Shi, [b] Shu Chen, [c] Zhenwei Zhu,*[d] and Wen Wan*[ae]

[a]*Materials Genome Institute, Shanghai University, Shanghai 200444, China. E-mail: tu_lan@shu.edu.cn, wwan@shu.edu.cn*
[b]*School of Materials Science and Engineering, Beijing Key Laboratory of Environmental Science and Engineering ,Beijing Institute of Technology, Beijing 100081, China.*
[c]*Terahertz Technology Innovation Research Institute, Shanghai Key Lab of Modern Optical System, University of Shanghai for Science and Technology, Shanghai 200093, China.*
[d]*Chemical Defense Institute, Beijing 100083, China. E-mail: zwzhu@stu.xmu.edu.cn*
[e]*State Key Laboratory of Advanced Refractories, Shanghai University, Shanghai, 200444, China.*

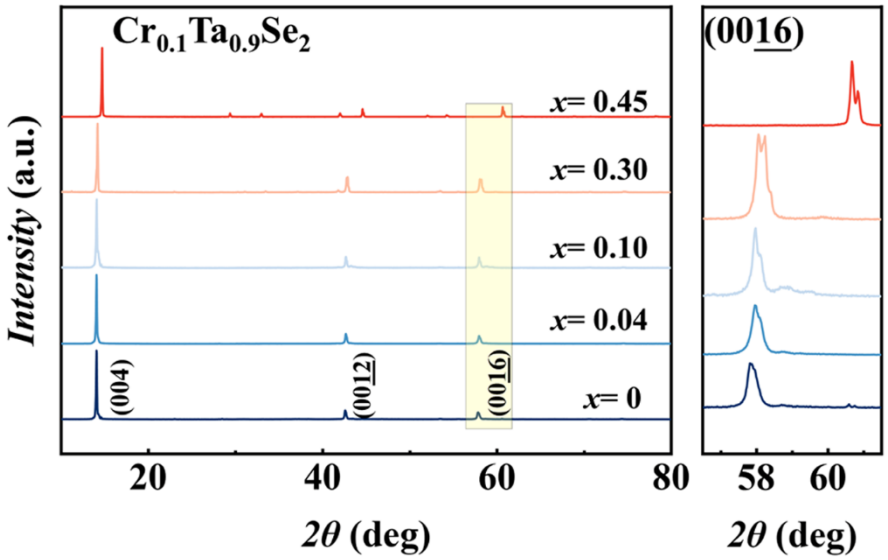

Fig. S1 As-grown $Cr_xTa_{1-x}Se_2$ polycrystalline and their structural evolution with x. The polycrystalline structure evolution on $Cr_xTa_{1-x}Se_2$ ($0 \leq x \leq 0.45$), the change on original structures of $TaSe_2$ can be seen after $x = 0.04$.

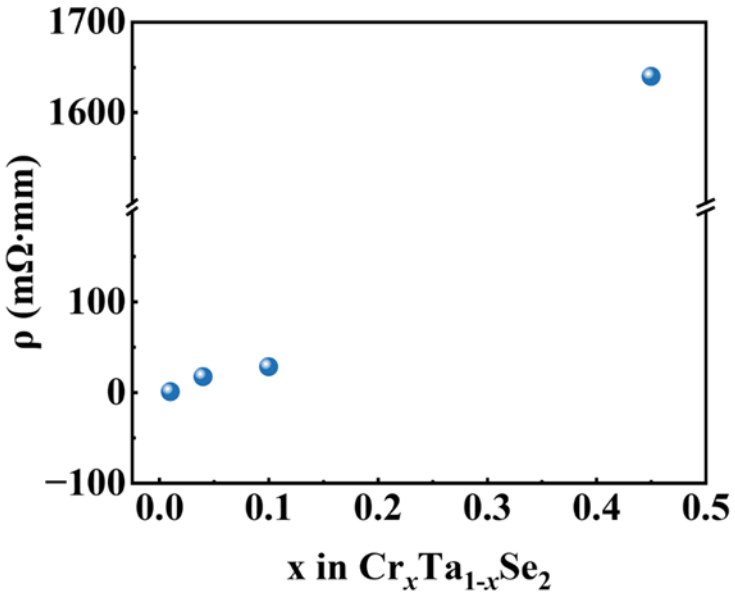

Fig. S2 Evolution of electrical resistivity in $Cr_xTa_{1-x}Se_2$ with x (25℃). Excessive Cr doping results in a drastic degradation of the electrical conductivity.

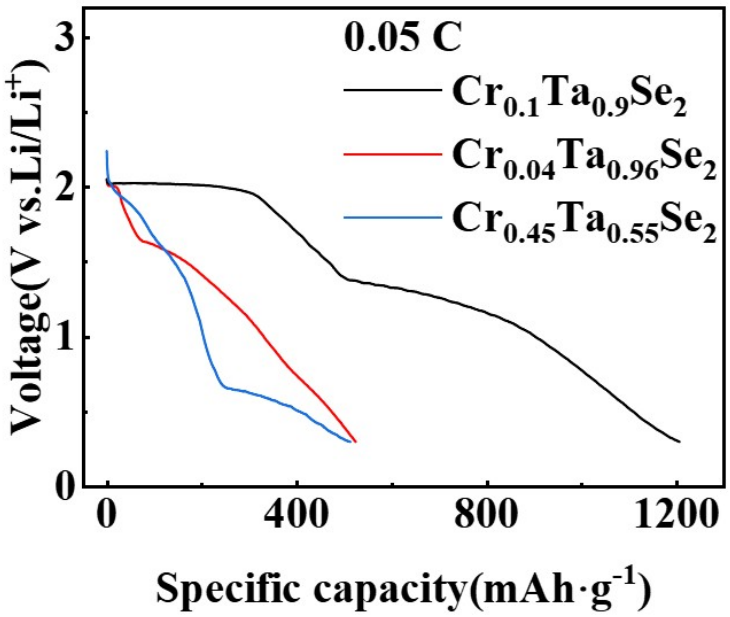

Fig. S3 Electrochemical performance of LIBs using $Cr_xTa_{1-x}Se_2$ as electrode materials: specific capacity versus voltage profiles at specific Cr doping contents and the resultant discharge capacities.

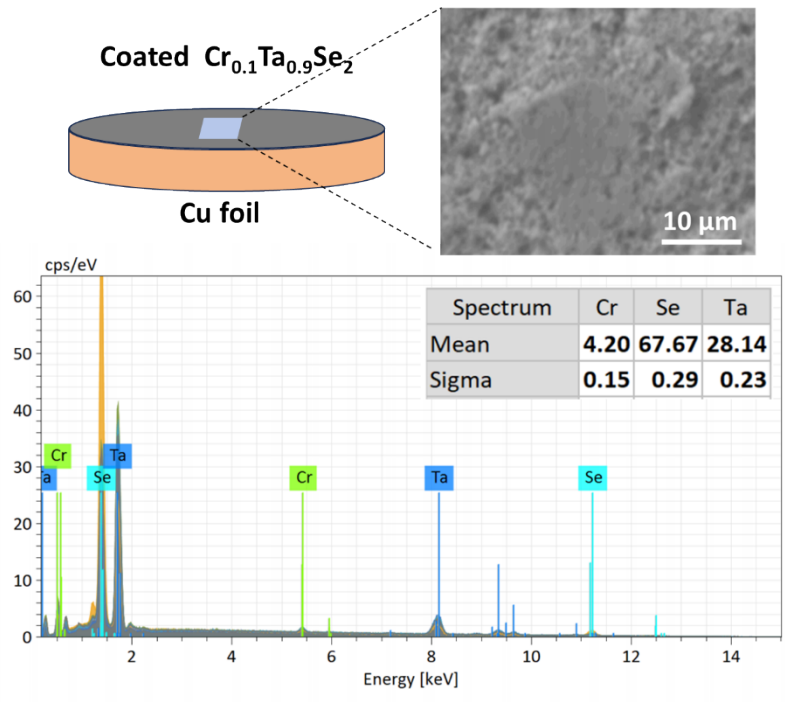

Fig. S4 Reconfirmation of the proportion of elemental components after coating of $Cr_{0.1}Ta_{0.9}Se_2$ on Cu foils by SEM and EDS measurements before each LIB testing. The corresponding atomic ratios are shown as 4.20%, 28.14%, and 67.67% for Cr, Ta, and Se, respectively, which are consistent with the proportion of as-grown samples.

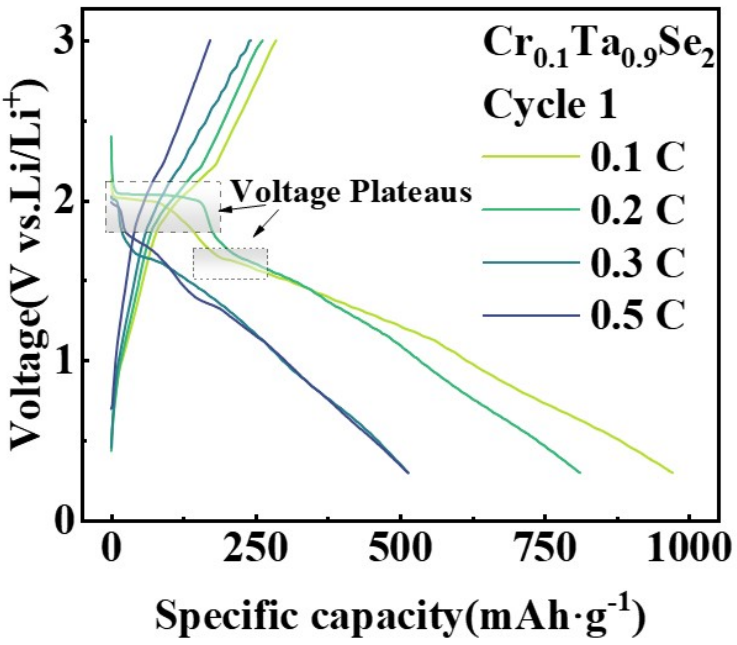

Fig. S5 Electrochemical evaluation of $Cr_{0.1}Ta_{0.9}Se_2$ as an electrode material: Voltage versus specific capacity profiles for the initial cycle measured at multiple charge-discharge rates.

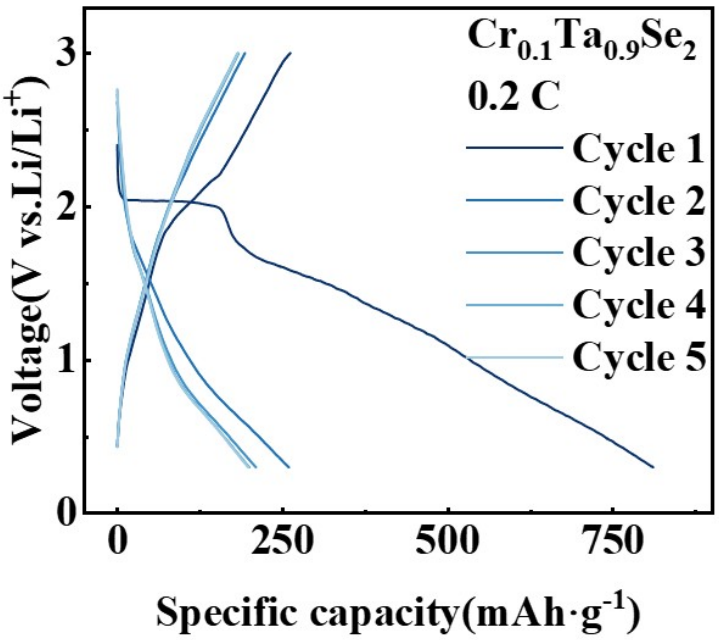

Fig. S6 Electrochemical performance of $Cr_{0.1}Ta_{0.9}Se_2$ as an electrode material: Voltage versus capacity profiles for the first five galvanostatic cycles tested at a current rate of 0.2 C.

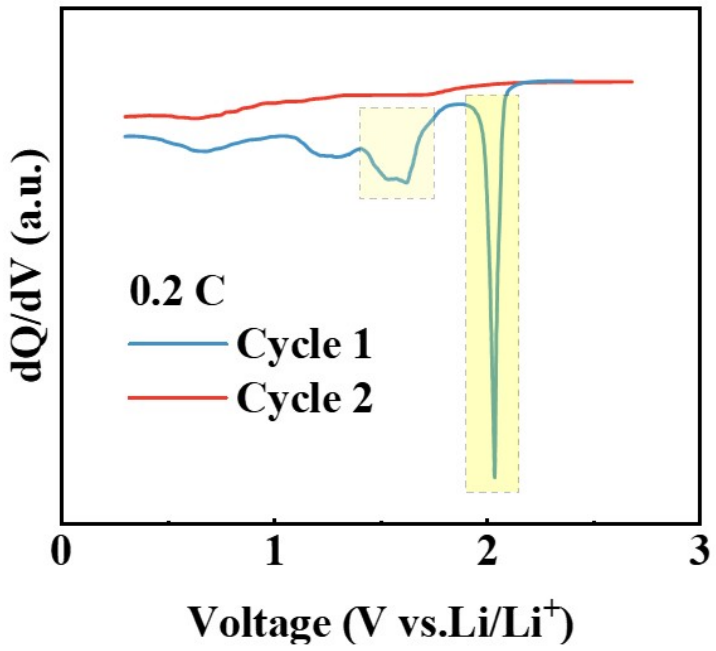

Fig. S7 Differential capacity curves of the first-cycle and second-cycle discharge profiles at a rate of 0.2C. Two well-defined voltage plateaus are observed in the first-cycle discharge profiles.

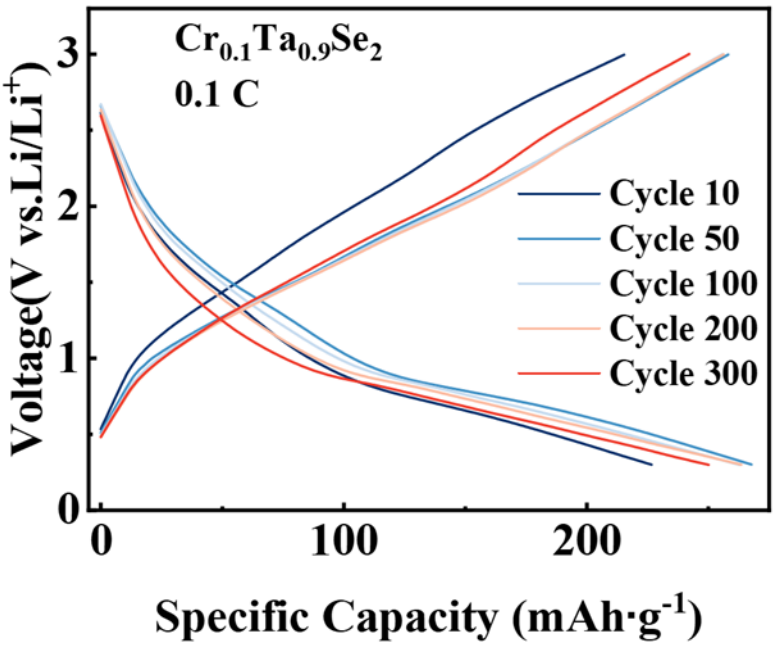

Fig. S8 Charge-discharge curves of $Cr_{0.1}Ta_{0.9}Se_2$ at 0.1 C rate for the 10th, 50th, 100th, 200th, and 300th cycles.

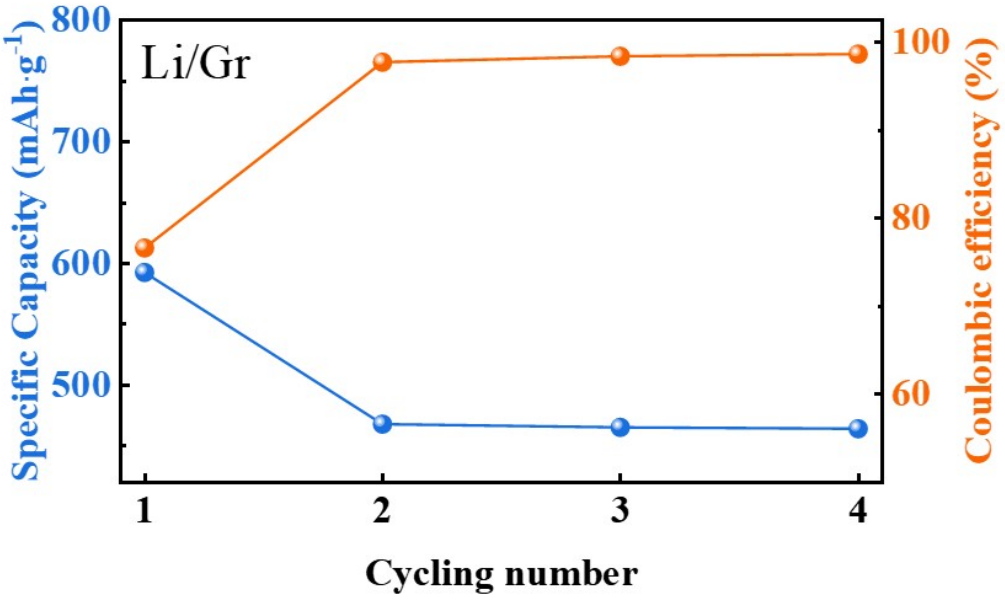

Fig. S9 Cycle number versus specific discharge capacity and coulombic efficiency curves of a graphite/Li half-cell.

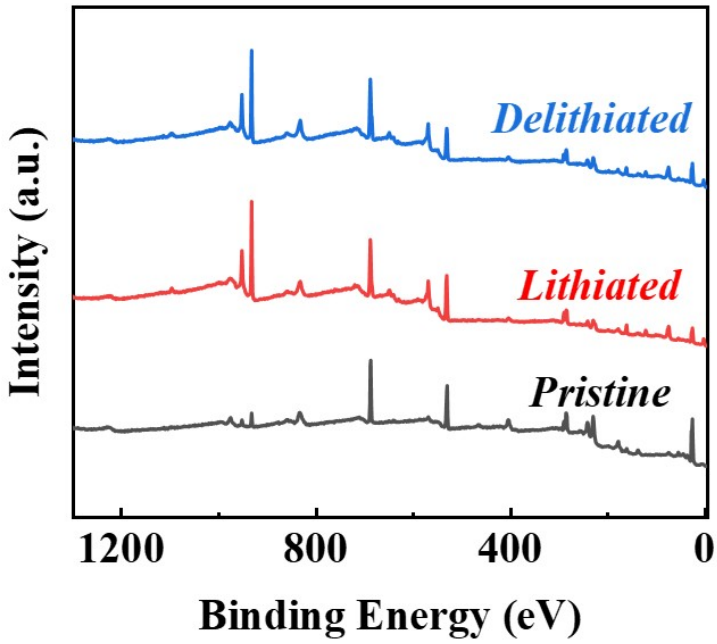

Fig. S10 Survey scan of XPS spectra on pristine, lithiated, and delithiated $Cr_{0.1}Ta_{0.9}Se_2$ electrode, respectively.

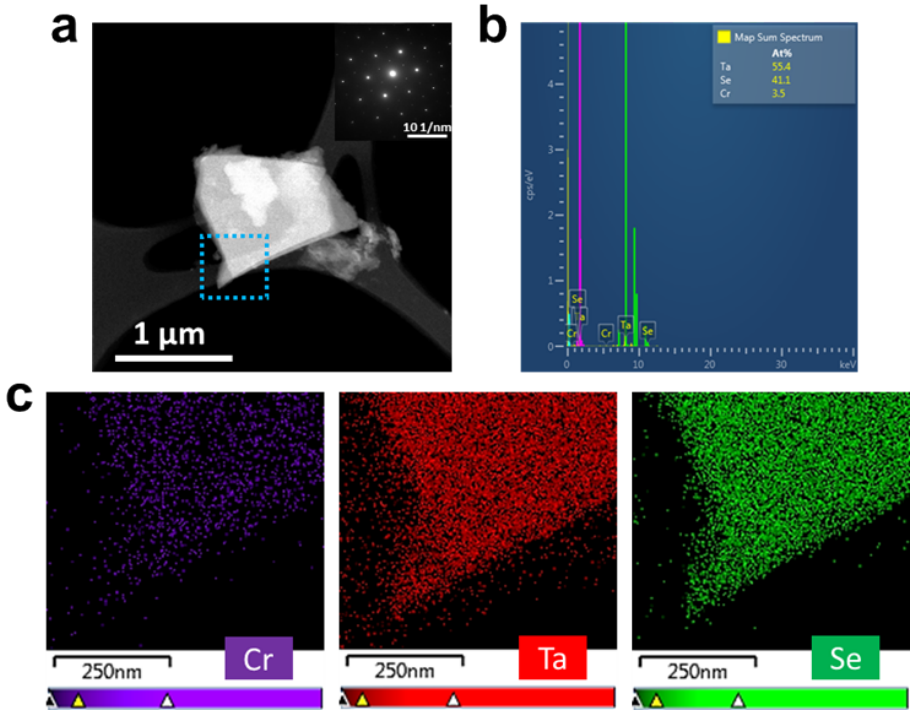

Fig. S11 Selected area electron diffraction (SAED) and energy-dispersive spectroscopy (EDS) measurements on the flakes used as the electrode material after the first two charge-discharge cycles. (a) The typical morphology of one flake with sharp boundaries of the electrode material. Its SAED patterns are also displayed on the upper-right corner, revealing a robust crystallinity after electrochemical reactions. (b) The EDS statistical analysis on the framed area of the flake in (a), showing element proportions as 55.4%, 41.1%, and 3.5% for Ta, Se, and Cr, respectively, indicates the escaping of both Cr and Se species from the lattice. (c) The EDS mapping for Cr, Ta, and Se on the framed area in (a), exhibiting uniform Cr, Ta, and Se distributions in this flake.